Non-diverging analytical expression for the sensitivity of converging SPECT collimators

Van Roosmalen, Jarno; Goorden, Marlies C.

DOI
10.1088/1361-6560/aa6646

Publication date
2017

Document Version
Accepted author manuscript

Published in
Physics in Medicine and Biology

Note

Non-diverging analytical expression for the sensitivity of converging SPECT collimators

Jarno van Roosmalen[1], **Marlies C Goorden**[1]

[1] Section of Radiation, Detection and Medical Imaging, Applied Sciences, Delft University of Technology, Mekelweg 15, 2629 JB Delft, The Netherlands

E-mail: j.vanroosmalen@tudelft.nl

Abstract. Accurate analytical expressions for collimator resolution and sensitivity are important tools in the optimization of SPECT systems. However, presently known expressions for the sensitivity of converging collimators either diverge near the focal point or focal line(s), or are only valid on the collimator axis. As a result, these expressions are unsuitable to calculate volumetric sensitivity for e.g. short-focal length collimators that focus inside the object to enhance sensitivity. To also enable collimator optimization for these geometries, we here present non-diverging sensitivity formulas for astigmatic, cone beam and fan beam collimators that are applicable over the full collimator's field-of-view. The sensitivity was calculated by integrating previously derived collimator response functions over the full detector surface. Contrary to common approximations, the varying solid angle subtended by different detector pixels was fully taken into account which results in a closed-form non-diverging formula for the sensitivity. We validated these expressions using ray-tracing simulations of a fan beam and an astigmatic cone beam collimator and found close agreement between the simulations and the sensitivity expression. The largest differences with the simulation were found close to the collimator, where sensitivity depends on the exact placement of holes and septa, while our expression represents an average over all possible placements as is common practice for analytical sensitivity expressions. We checked that average differences between the analytical expression and simulations reduced to less than 1% of the maximum sensitivity when we averaged our simulations over different septa locations. Moreover, we found that our new expression reduced to the traditional diverging formula under certain assumptions. Therefore, the newly derived sensitivity expression may enable the optimization of converging collimators for a wide range of applications, in particular when the focal area is close to, or in, the object of interest.

Submitted to: *Phys. Med. Biol.*

1. Introduction

The use of converging collimators in Single Photon Emission Computed Tomography (SPECT) has already been proposed since the 1980s (Jaszczak et al., 1979; Tsui et al., 1986; Jaszczak et al., 1986, 1988; Gullberg, Christian, Zeng, Datz and Morgan, 1991; Gullberg, Zeng, Christian, Tsui and Morgan, 1991). Such converging collimators, in which the hole's axes converge to a focal line (fan beam), a focal point (cone beam), or multiple focal lines (astigmatic), are advantageous for increasing photon yield or sensitivity over that of parallel hole collimators if the dimensions of the target object or organ are smaller than those of the gamma detector. Additionally, combinations of different converging collimators, e.g. combined half-cone beam and fan beam collimation have been investigated for high-sensitivity SPECT (Li et al., 1996; Kamphuis and Beekman, 1998; Beekman et al., 1998; Ter-Antonyan et al., 2009). Because the sensitivity of converging collimators is highest near the focal line(s) or point, various researchers have proposed to use short focal length cone beam collimators with focus inside the object of interest, e.g. Hawman and Haines (1994); Walrand et al. (2002); Park et al. (2003, 2005); van Roosmalen et al. (2015). The increased sensitivity due to focusing inside the object may also reduce noise in reconstructed images induced by attenuation as was shown by Kijewski et al. (1997) and may benefit SPECT systems equipped with transmission sources (SPECT/Transmission Computed Tomography (TCT) systems) by increasing the number of transmission counts. These systems based on fan beam collimators can have transmission line or point sources at the focal line (Kemp et al., 1995; Beekman et al., 1998), or use virtual point sources at the focal point of a cone beam collimator (Manglos et al., 1992; Beekman, 2001).

An important tool in SPECT and SPECT/TCT system design is the use of accurate analytical expressions for collimator resolution and sensitivity. However, common expressions for the sensitivity of converging collimators (Metz et al., 1980; Tsui and Gullberg, 1990) inappropriately diverge near the collimator's focus. Moreover, the divergence scales with $1/r^n$, with r being the distance from the focus and $n = 1$ for fan beam and $n = 2$ for cone beam collimators, making the expressions non-integrable around the focus. Thus, when calculating volumetric collimator sensitivity over a region containing the focus, one cannot circumvent the singularity at the focus by taking points just outside of the focus location. This is particularly problematic for designing systems that exploit the increased sensitivity near the focus such as the short-focal-length collimator geometries mentioned above.

To circumvent the issue of diverging analytical expressions, other methods for determining the sensitivity have been used in optimization studies. For example measurements on physical collimators (Jaszczak et al., 1988; Li et al., 1996), extensive Monte Carlo or raytracing simulations (Jaszczak et al., 1986) can give accurate estimates. However, these methods are computationally expensive, and do thus not allow for quick evaluation of a large number of design parameters, or fast analytical optimization based on the expressions themselves. At the same time, analytical expressions have often been used for optimizing other collimator types, e.g. Lowe et al. (2002); Gunter (2004); Rentmeester et al. (2007); Goorden et al. (2008); Weinmann et al. (2009), and for an overview see Van Audenhaege et al. (2015). Therefore, the availability of accurate non-diverging expressions is expected to enable easier and faster optimization of converging collimators for a wide range of geometries.

Non-diverging expressions were previously derived by Accorsi and Metzler (2006),

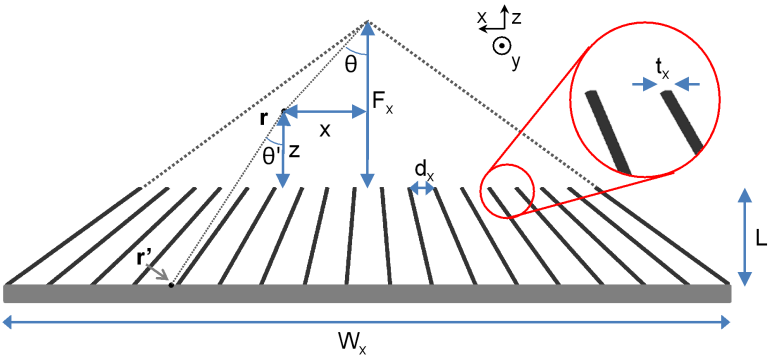

Figure 1. Schematic cross-section through a converging collimator with parameters used in this paper indicated.

but only for the on-axis sensitivity of converging collimators. In this work, we present new sensitivity formulas that are valid over the whole field-of view, and we validate these using raytracing software.

2. Methods

2.1. General collimator theory

We start here with introducing the parameters and with repeating the standard collimator theory on which our derivation is based. The collimator model and some of the parameters describing it are shown in figure 1. Assuming the z-axis to be perpendicular to the detector, we define F_x, F_y, d_x, d_y, t_x, and t_y to be the focal lengths, hole widths and septal thicknesses in x- and y-directions respectively while L is the collimator thickness. Both the hole widths and septal widths are defined at the object side of the collimator. Along the z-direction they both increase by the same factor which depends on the amount of focusing. We assume that the detector has a rectangular shape and that it extends from $x = -W_x/2$ to $x = W_x/2$ and from $y = -W_y/2$ to $y = W_y/2$.

Our derivation starts from the general collimator theory described in Metz et al. (1980) for parallel holes, which was extended in Tsui and Gullberg (1990) to cone beam collimators. Here we adopt the notation of the latter paper while throughout our expression we also allow for fan beam and astigmatic collimators.

We look at the response to a point source located at (x, y, z). The perpendicular projection of the source on the detector plane is represented by $\mathbf{r} = (x, y)$. Note that this is a two-dimensional coordinate as it represents a point on the detector. The following equation describes the fluence ϕ $[m^{-2}]$ of photons detected at point $\mathbf{r}' = (x', y')$ on the detector,

$$\phi(\mathbf{r}', \mathbf{r}, z) = \frac{k}{4\pi\,(z+L)^2} \cos^3\theta' A(\mathbf{r}', \mathbf{r}, z) \tag{1}$$

where k $[m^{-2}]$ is a proportionality factor which will be discussed later and $A(\mathbf{r}', \mathbf{r}, z)$ $[m^2]$ is the aperture function of the collimator at point $\mathbf{r}'$ on the detector. Moreover, in this expression, θ' is the angle between the z-axis and the vector connecting the

point source with the point $\mathbf{r}'$ on the detector as indicated in figure 1. It can thus be written as

$$\cos\theta' = \frac{z+L}{\sqrt{(z+L)^2 + |\mathbf{r}'-\mathbf{r}|^2}}. \tag{2}$$

The collimator aperture function $A(\mathbf{r}', \mathbf{r}, z)$ is determined from the aperture functions of a single hole $a_f(\mathbf{r}'')$ and $a_b(\mathbf{r}'')$ respectively at the front and at the back of the collimator, which are one for lateral positions $\mathbf{r}'' = (x'', y'')$ inside the collimator hole and zero outside of the hole. If one projects the front and back apertures from the source position onto the detector then the size of the overlap between these projections determines the fraction of photons that can pass through the collimator hole. Now the common way to calculate the sensitivity, is to continuously translate a single hole over the detector to arrive at an average sensitivity which does not depend on the exact position of the septa. For the general case of astigmatic collimators with holes on a lattice it was shown that $A(\mathbf{r}', \mathbf{r}, z)$ can be written in the following way (Tsui and Gullberg, 1990; Formiconi, 1998)

$$A(\mathbf{r}', \mathbf{r}, z) = \int_{-\infty}^{\infty} a_f(-\boldsymbol{\sigma}) a_f\left(\mathbf{r}_T(\mathbf{r}', \mathbf{r}, z) - \boldsymbol{\sigma}\right) \mathrm{d}\boldsymbol{\sigma}, \tag{3}$$

where $\boldsymbol{\sigma} = (\sigma_x, \sigma_y)$, $\mathbf{r}_T(\mathbf{r}', \mathbf{r}, z) = (x_T(x, x', z), y_T(y, y', z))$ and

$$x_T(x, x', z) = \frac{L(F_x - z)}{(F_x + L)(z + L)} x' - \frac{L}{z+L} x, \tag{4}$$

$$y_T(y, y', z) = \frac{L(F_y - z)}{(F_y + L)(z + L)} y' - \frac{L}{z+L} y. \tag{5}$$

Note that these equations thus average out the details of the exact location of the individual septa and holes (Tsui and Gullberg, 1990; Formiconi, 1998). Here σ represents a shift of the hole parallel to the detector plane, to average the response over all possible hole locations. Moreover, $\mathbf{r}_T$ represents the vector on the collimator surface between the line from the focus to the point $\mathbf{r}'$ on the detector and the line from the source to $\mathbf{r}'$ (see figure A1 in the appendix for an illustration).

In our derivation we assume rectangular holes (in the discussion we come back to other hole shapes) and one thus has an aperture function $a_f(\boldsymbol{\sigma}) = 1$ if $|\sigma_x| < d_x/2$ and $|\sigma_y| < d_y/2$. The collimator's aperture function can then be calculated and it reads

$$A(\mathbf{r}', \mathbf{r}, z) = (d_x - |x_T|)\,(d_y - |y_T|)\,, \tag{6}$$

for $|x_T| < d_x$ and $|y_T| < d_y$ and 0 otherwise. To determine the sensitivity, the flux has to be integrated over the detector plane. One can show that in order to arrive at a physically meaningful sensitivity, one has to set the proportionality constant $k^{-1} = (d_x + t_x)\,(d_y + t_y)$ (Tsui and Gullberg, 1990). With these definitions, the flux in (1) is fully defined, and the sensitivity is given by

$$\begin{aligned} S &= \int_{-W_x/2}^{W_x/2} \int_{-W_y/2}^{W_y/2} \mathrm{d}x' \mathrm{d}y' \phi(\mathbf{r}', \mathbf{r}, z) \\ &= \frac{F_x + L}{|F_x - z|} \frac{F_y + L}{|F_y - z|} \frac{1}{L^2 4\pi\,(d_x + t_x)\,(d_y + t_y)} \cdot \\ &\quad \int_{\chi_{-1}}^{\chi_1} \int_{\xi_{-1}}^{\xi_1} \mathrm{d}x_T \mathrm{d}y_T (d_x - |x_T|)(d_y - |y_T|) \cos^3\theta' \end{aligned} \tag{7}$$

Here, the integration limits χ_{-1}, χ_1, ξ_{-1} and ξ_1 can be calculated by

$$\chi_i = \min\left\{\max\left[-d_x, -\frac{L|x|}{L+z} + \frac{1}{2}iW_x\left|\frac{L(F_x-z)}{(F_x+L)(L+z)}\right|\right], d_x\right\}, \quad (8)$$

$$\xi_i = \min\left\{\max\left[-d_y, -\frac{L|y|}{L+z} + \frac{1}{2}iW_y\left|\frac{L(F_y-z)}{(F_y+L)(L+z)}\right|\right], d_y\right\}. \quad (9)$$

Note that the integration limits are coordinates defined on the front surface of the collimator, where $\mathbf{r}_T$ was defined (see figure A1). The response that is being integrated is for a single moving hole. Therefore, the limits in (8) and (9) are usually from -d_x to d_x (or $-d_y$ to d_y), except when the hole is partly over the edge of the finite detector, then the integration range becomes smaller.

2.2. Conventional diverging expression

Now the usual approach is to approximate θ' with θ (the angle between the z-axis and the line from the focus to $\mathbf{r}$, see figure 1). This approximation is based on the assumption that the detector response to a point source is narrow, i.e. gamma photons from the source can only reach the detector through a few holes. In this case the $\cos^3\theta'$ can be approximated by $\cos^3\theta$ in (7) and taken out of the integral as it is now a constant. Furthermore, in these traditional derivations the finite detector size is not taken into account. Under these assumptions, the integral is straightforward to perform and one finds the usual diverging formula for sensitivity, c.f. Moyer (1974); Jaszczak et al. (1986) or Formiconi (1998)

$$S_{\text{div}} = \cos^3\theta \frac{1}{4\pi}\frac{F_x+L}{|F_x-z|}\frac{F_y+L}{|F_y-z|}\frac{d_x^2 d_y^2}{L^2(d_x+t_x)(d_y+t_y)}. \quad (10)$$

Using basic trigonometry one can write $\cos\theta = 1/\sqrt{1+x^2/(F_x-z)^2+y^2/(F_y-z)^2}$.

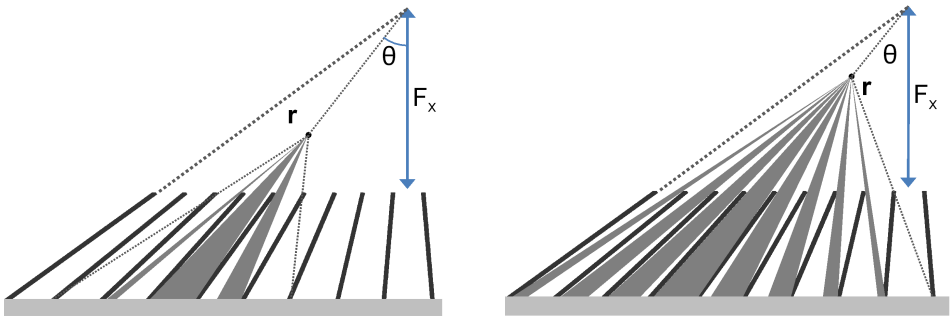

(a) (b)

Figure 2. Schematic representation of the holes that contribute to the sensitivity for two different point source locations. Dotted lines illustrate paths that are blocked by the collimator. (a) Point source located away from the focus resulting in a narrow detector response to which only a few holes contribute. (b) Point source located close to the focus having a wide detector response as paths from the source can reach the detector through many holes.

2.3. Non-diverging expression

The reason that the common sensitivity expressions diverge near the focal point/ lines is due to the fact that the assumptions stated in section 2.2 do not hold close to the focal point, as close to the focal point many holes "see" the source and the response is not narrow, see figure 2. Thus, for these non-narrow responses one cannot approximate θ' with θ and the $\cos^3\theta'$ term has to be included inside the integral as it varies over the detector. In (2) we already provided an exact expression for $\cos\theta'$ in terms of $\mathbf{r}$ and $\mathbf{r}'$, which can be substituted in (7).

Moreover, near the focal point or line the finite detector size starts to play a role; when a source is placed in the focal point all holes transmit gamma photons from the source and thus the sensitivity reduces to the solid angle subtended by the detector plane, corrected for the fact that no signal is detected underneath the septa. As the solid angle of a finite detector is usually significantly different from that of an infinite detector, the detector size should play a role for all points in a region around the focus.

Therefore, to arrive at a realistic expression for sensitivity which is also valid near the collimator's focus, we have to evaluate the full integral of (7) without any approximation. In principle, this evaluation consists of performing standard integrals, that can e.g. be found in textbooks like Gradshteyn and Ryzhik (2014). Note that the integration limits in (7) are complicated expressions given in (8) and (9), so especially the second integration is quite complex involving many terms. Therefore, the resulting expression becomes very complicated and very lengthy and we had to perform extensive simplification in order to arrive at a tractable form that can be presented in a paper and that other researchers can incorporate into their collimator optimization code. In the supplementary information we provide the results of the first integration and the simplification applied to this intermediate result. The mentioned simplifications consisted of exact algebraic manipulation of the (intermediate) expressions, in order to arrive at a representable formula, but they did not involve any approximations. For example, we identified several frequently occurring sub-expressions which could be replaced by a single variable or function. All algebraic manipulations of expressions were supported by the computer program Mathematica (Wolfram Research Inc.). The Mathematica file is available in the supplementary information.

2.4. Validation

We validate the results using our raytracing software that we developed and validated with Monte Carlo simulations (Wang et al., submitted). This raytracing code uses a voxel based model (0.05 mm voxels in this paper) of the collimator, where each voxel consists of either air, or collimator material. The voxel size was chosen to be sufficiently small to accurately model the septa, i.e. a small test gave sensitivity differences of a few percent compared to results with much smaller voxels. The software determines the path length through materials from the source to each of the 36 million detector pixels with a Siddon-like raytracing algorithm. The algorithm follows a ray from source to a detector pixel through the collimator. In every voxel the path length of the ray through the voxel is calculated and multiplied by the linear attenuation coefficient. We use Siddon's efficient algorithm to compute this path length (Siddon, 1985). The accumulated probability that the ray is attenuated in the collimator combined with a geometrical factor gives the final probability that a photon emitted from the source

is detected at this specific pixel. The geometrical factor is the solid angle of the pixel extended towards the source (i.e. the probability that the pixel would detect gamma photons from the source if no collimator would be present). We modelled the detector with 0.05 x 0.05 mm pixels, to accurately describe the exact response of the holes, without suffering from discretization errors.

For testing our expression, modelling of the detector response has been turned off as is common. To validate the collimator response formula, the geometrical response of the collimator was calculated without modelling penetration of gamma rays through the septa. Therefore, this is initially also turned off in our raytracing software to first test for agreement in this ideal case. As in our derivation, holes are assumed to be rectangular in the simulation. We consider two collimators in our validation. The first is a fan beam collimator with $d_x = d_y = 1.4$ mm, $t_x = t_y = 0.2$ mm, $L = 27$ mm, $F_x = 45$ mm. For fan beam collimators, F_y is set to ∞. The second collimator we use for validation is an astigmatic cone beam collimator with $d_x = 1.4$ mm, $d_y = 1.1$ mm, $t_x = 0.2$ mm, $t_y = 0.3$ mm, $L = 27$ mm, $F_x = 45$ mm and $F_y = 60$ mm. In both cases the detector is assumed to be 300 mm by 300 mm.

It is expected that close to the collimator the sensitivity will strongly depend on the precise location of the septa and holes. However, as it is generally undesirable to have complicated sensitivity expressions containing the exact locations of the septa, we based the analytical derivation on averaging over all possible configurations, as is common to do. To be able to validate the expression against this assumption, we shifted the septa in our voxelized collimator model in 10 steps of 0.16 mm, for both x and y directions for the fan beam example. For the cone beam example we use steps of 0.16 and 0.14 mm for x and y respectively. This results in 100 unique collimator configurations, which were each simulated using our raytracer. The average sensitivity is then reported, as are the results of a single configuration to illustrate the difference.

Moreover, we investigated if we can use the usual approach of incorporating septal penetration by an effective hole length, $L_e = L - 2/\mu$ (Mather, 1957; Moyer, 1974). To test how accurate this approximation is, we replace L by L_e in our formulas and include penetration in our raytracing code for the same collimators as described above. We assume tungsten septa with $\mu = 3.39$ mm^{-1} for 140 keV gamma rays.

2.4.1. Volumetric Sensitivity. To see the importance of the new expressions for volumetric sensitivity calculations we test an example loosely based on the brain SPECT system of Park et al. (2005). We assume a 300 mm by 300 mm detector with a collimator with $L = 24$ mm, $d_x = d_y = 1.1$ mm and $t_x = t_y = 0.16$ mm. The mean sensitivity is calculated for a sphere with a diameter of 200 mm, located 50 mm from the collimator surface (mimicking a 150 mm radius of rotation). We will evaluate the sensitivity for a range of focal lengths from 150 mm (focus in the centre of the sphere) till 400 mm (focus outside sphere).

3. Results

3.1. Analytical expression

After integrating (7) and extensive simplification, we arrived at the following closed-form expression for the sensitivity

$$S = \frac{L^2}{4\pi}\frac{1}{d_x+t_x}\frac{1}{d_y+t_y}\frac{|F_x-z|}{F_x+L}\frac{|F_y-z|}{F_y+L}\sum_{i=-1}^{1}\sum_{j=-1}^{1} S_{i,j} \tag{11}$$

The term $S_{i,j}$ is given by

$$\begin{aligned} S_{i,j} = (-1)^{i+j}\,(2-|i|)\,(2-|j|)\,(i-(1+i)\,U\,(\chi_1))\,(j-(1+j)U(\xi_1)) \\ \left[-\sqrt{1+b_x^2(i)+b_y^2(j)} + a_x(i)a_y(j)\arctan\left(\frac{b_x(i)b_y(j)}{\sqrt{1+b_x^2(i)+b_y^2(j)}}\right)\right. \\ -a_x(i)\ln\left(-b_x(i)+\sqrt{1+b_x^2(i)+b_y^2(j)}\right) \\ \left.-a_y(j)\ln\left(-b_y(j)+\sqrt{1+b_x^2(i)+b_y^2(j)}\right)\right] \end{aligned} \tag{12}$$

where U denotes the unit step function ($U(x)=1$ for $x>0$ and $U(x)=0$ for $x\leq 0$). Furthermore, the constants a_x, a_y, b_x and b_y read (for $i=-1,1$ and $j=-1,1$)

$$a_x(i) = \frac{F_x+L}{F_x-z}\frac{d_x}{L}\text{sign}(\chi_i) + \frac{|x|}{F_x-z}, \quad a_y(j) = \frac{F_y+L}{F_y-z}\frac{d_y}{L}\text{sign}(\xi_j) + \frac{|y|}{F_y-z}, \tag{13}$$

$$b_x(i) = \frac{F_x+L}{F_x-z}\frac{\chi_i}{L} + \frac{|x|}{F_x-z}, \qquad b_y(j) = \frac{F_y+L}{F_y-z}\frac{\xi_j}{L} + \frac{|y|}{F_y-z} \tag{14}$$

while for $i=0$ respectively $j=0$, we have

$$a_x(0) = b_x(0) = |x|/(F_x-z), \qquad a_y(0) = b_y(0) = |y|/(F_y-z). \tag{15}$$

The finite detector size is incorporated in χ_i and ξ_j which were defined previously in (8) and (9). Although this is still a rather complicated expression, it can easily be incorporated in a computer program to quickly calculate the sensitivity for different collimators in e.g. an optimization study.

3.2. Special cases

It is important to show that under the right assumptions the well known and previously published formulas can be recovered. The traditional diverging formula was derived under the assumption that the detector has an infinite size and that $\theta' \approx \theta$ (i.e. the detector response is narrow, see figure 2 and section 2.3). For an infinite detector, $W_x = W_y = \infty$ and this gives $\chi_i = id_x$ and $\xi_i = id_y$. Furthermore, we assume that $|F_x - z| \gg d_x(F_x+L)/L$ and $|F_y - z| \gg d_y(F_y+L)/L$. This corresponds to assuming that the vertical distance from the focal point/line ($|F_x-z|$), is much larger than the back projected size of a hole ($d_x(F_x+L)/L$) along the same vertical axis. First order expansion in $d_x(F_x+L)/(L|F_x-z|)$ and $d_y(F_y+L)/(L|F_y-z|)$ of (11) gives

$$S \approx \frac{1}{4\pi}\frac{F_x+L}{|F_x-z|}\frac{F_y+L}{|F_y-z|}\frac{d_x^2 d_y^2}{L^2(d_x+t_x)(d_y+t_y)}\left(\left(\frac{x}{F_x-z}\right)^2 + \left(\frac{y}{F_y-z}\right)^2 + 1\right)^{-\frac{3}{2}}. \tag{16}$$

Using the expression for $\cos\theta$, defined in section 2.2 we can rewrite this as (10) (duplicated here for convenience)

$$S_{\text{div}} = \cos^3\theta \frac{1}{4\pi} \frac{F_x + L}{|F_x - z|} \frac{F_y + L}{|F_y - z|} \frac{d_x^2 d_y^2}{L^2(d_x + t_x)(d_y + t_y)}.$$

It is also of interest to consider sensitivity at the focal point of a cone beam collimator. This is done by first setting $x = y = 0$, and $F_y = F_x$ and then taking the limit $z \to F_x$. Setting $x = y = 0$ means the first term with $|x|$ and $|y|$ respectively in χ_i and ξ_i drops, and the second term drops out of $a_x(i)$, $a_y(j)$, $b_x(i)$ and $b_y(j)$ in (13), (14) and $a_x(0) = a_y(0) = b_x(0) = b_y(0) = 0$. The $a_x(i)$, $a_y(j)$, $b_x(i)$ and $b_y(j)$ terms diverge for $i, j \neq 0$ in the limit $F_x - z \to 0$, but the divergence is cancelled by the $|F_x - z|$ from the pre-factor in (11). All the terms with either $i = 0$ or $j = 0$ are 0 in (12), leaving us with 4 equal terms that add up to

$$S_{\text{foc}} = \frac{d_x d_y}{\pi(d_x + t_x)(d_y + t_y)} \arctan\left(\frac{W_x W_y}{2\,(F_x + L)\sqrt{4\,(F_x + L)^2 + W_x^2 + W_y^2}} \right), \tag{17}$$

which is just the solid angle of the detector corrected for the presence of septa (cf. (29) from Accorsi and Metzler (2006)). Note that for an infinite detector the arctan term becomes $\arctan(\infty) = \pi/2$ and so the sensitivity reduces to $d_x d_y/(2(d_x + t_x)(d_y + t_y))$ which in the limit of septal thickness going to 0, reduces to $1/2$ as expected for a single infinite detector.

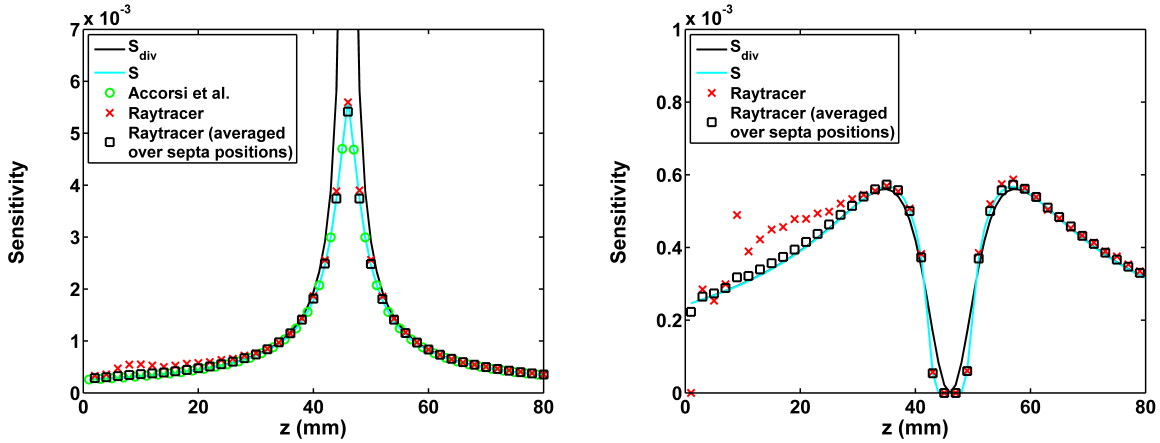

Figure 3. Comparison of analytically calculated sensitivity (cyan solid line) for fan beam collimator with raytracing simulations. Simulation results for one particular position of the septa (red crosses) and an average over 100 different septa positions (black squares) are provided. Sensitivity given by the traditional diverging formula (black solid line) and a previously derived on-axis non-diverging formula of Accorsi and Metzler (2006) (green circles) are shown as well. (a) For $x = 0$ mm and $y = 0$ mm, (b) idem for sensitivity at $x = 8$ mm, $y = 0$ mm.

3.3. Validation by raytracing

In figure 3 and figure 4 we compared the sensitivity given by (11) with raytracing simulations for the fan beam and cone beam example respectively. As explained in section 2.4, in our raytracing simulation we generated 100 different collimator configurations in which the location of the septa and holes was slightly different. Figure 3 shows the sensitivity averaged over these 100 configurations (black squares) and the sensitivity of one of these configurations (red crosses). The single configuration chosen is the one where a septum touches the collimator axis (one side of septum at $x = 0$, $y = 0$). As a reference we also plotted the conventional diverging expression provided in (10) and we showed the results of the earlier derived on-axis formula from Accorsi and Metzler (2006) for the on-axis plots.

Figure 3a and figure 4a show the sensitivity profiles along the collimator axis (i.e. $x = 0$ and $y = 0$ mm), where the earlier expression derived by Accorsi et al. should also be valid. We indeed find very close agreement among S from (11), the ray-tracing simulation average over different septa locations and Accorsi's expression. We reported all differences between the analytical expressions and the simulations (averaged over the plotted profiles) as percentages of the maximum sensitivity obtained with that collimator in the simulation. For the fan beam collimator, the average and the maximum absolute difference between (11) and the averaged raytracing simulation are 0.5% and 4.3% respectively, as tabulated in table 1. For the cone beam collimator, the average absolute difference between (11) and the averaged raytracer result is 0.7% of the maximum. The expression from Accorsi and Metzler (2006) was only derived on the collimator axis, where it agrees very well with (11). For both collimators the relative difference is everywhere less than 1/10 000th. The divergence of the traditional expression at the focal line is also clear from the image. In fact we see that in a region of 8 mm at either side of the focus, the error of (10) is more than 5%. This corresponds with the condition found in section 3.2 for the divergent formula to be valid, i.e. $|F_x - z| \gg d_x(F_x + L)/L = 3.7$ mm .

In figure 3b and figure 4b-4d, we plotted sensitivity obtained from the same expressions but now along lines off the collimator axis ($x = 8$ mm and $y = 0$ mm,

Table 1. Mean/Max (over $z = 0$ to $z = 80$ mm) absolute differences for sensitivity expressions (S from (11), S_{div} from (10), and the previously derived non-diverging expression from Accorsi and Metzler (2006)) compared to raytracing simulation, and expressed as percentage of maximum sensitivity along each line in the simulation.

Mean/Max Difference (%)	S		S_{div}		Accorsi *et al*	
Location (mm)	Fixed septa	Averaged over septa	Fixed septa	Averaged over septa	Fixed septa	Averaged over septa
Fan Beam						
$x = 0$, $y = 0$	1.4 / 4.3	0.5 / 4.3	∞ / ∞	∞ / ∞	1.4 / 4.3	0.5 / 4.3
$x = 8$, $y = 0$	0.6 / 4.4	0.1 / 0.5	0.7 / 3.5	0.3 / 4.1	N/A	N/A
Cone Beam						
$x = 0$, $y = 0$	0.9 / 6.0	0.7 / 5.6	∞ / ∞	∞ / ∞	0.9 / 6.0	0.7 / 5.6
$x = 8$, $y = 0$	0.4 / 5.5	0.3 / 5.4	∞ / ∞	∞ / ∞	N/A	N/A
$x = 0$, $y = 8$	0.3 / 3.4	0.2 / 3.7	∞ / ∞	∞ / ∞	N/A	N/A
$x = 8$, $y = 8$	0.1 / 1.1	0.1 / 0.4	0.4 / 3.4	0.4 / 3.4	N/A	N/A

$x = 0$ mm and $y = 8$ mm, and $x = y = 8$ mm respectively). Note that for the fan beam collimator in total only two images are shown due to symmetry considerations. As the cone beam collimator is astigmatic, no symmetry is expected. Along the off-axis lines in figure 3b and figure 4d (note that in figure 4b and figure 4c there is still a diverging point), the traditional sensitivity formula does not diverge and is better able to describe the sensitivity than on-axis. Like in the on-axis case, we found close

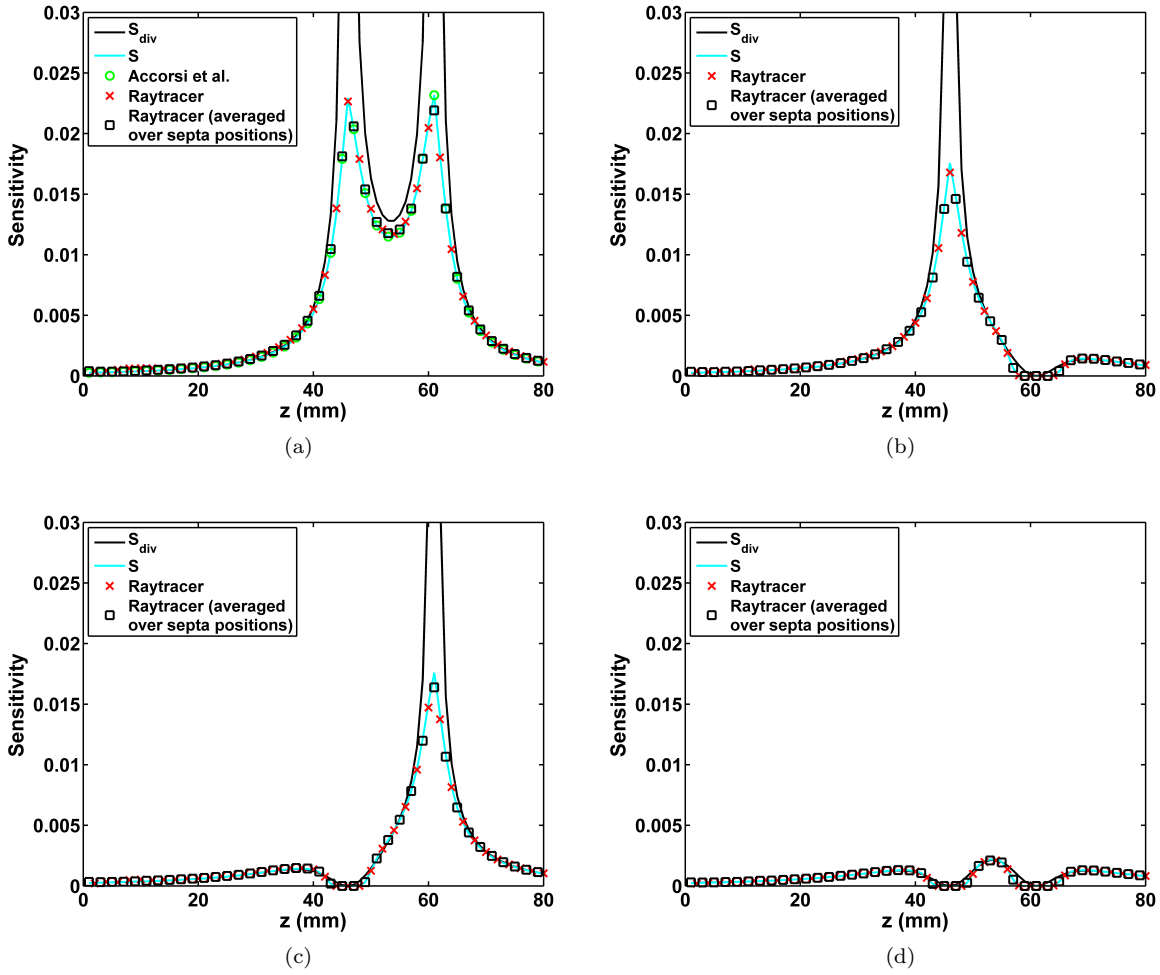

Figure 4. Comparison of analytically calculated sensitivity (cyan solid line) for astigmatic cone beam collimator with raytracing simulations. Simulations results for one particular position of the septa (red crosses), and an average over 100 different septa positions (black squares) are provided, as is the sensitivity given by the traditional diverging formula (black solid line). For on-axis results a previously derived on-axis non-diverging formula of Accorsi and Metzler (2006) (green circles) is shown. (a) For x =0 and $y = 0$, (b) idem for sensitivity at $x = 8$ mm, $y = 0$ mm, (c) idem for $x = 0$ mm, $y = 8$ mm (d) idem for $x = 8$ mm, $y = 8$ mm

.

Table 2. Mean/Max (over $z = 0$ to $z = 80$ mm) absolute difference between raytracing simulation with modelling of septa penetration and either (11) with the actual collimator length L or (11) with L replaced by the effective collimator length L_e expressed as percentage of maximum sensitivity along each line in the simulation.

Mean/Max Difference (%)	S With L		S With L_e	
Location (mm)	Fixed septa	Averaged over septa	Fixed septa	Averaged over septa
Fan Beam				
$x = 0$, $y = 0$	2.5 / 6.5	1.5 / 3.8	2.0 / 4.7	0.9 / 3.3
$x = 8$, $y = 0$	1.1 / 4.0	0.7 / 1.0	0.9 / 3.8	0.4 / 0.7
Cone Beam				
$x = 0$, $y = 0$	2.8 / 8.1	2.6 / 7.8	2.3 / 6.5	2.0 / 6.2
$x = 8$, $y = 0$	1.2 / 4.7	1.1 / 4.8	1.0 / 3.6	0.9 / 3.6
$x = 0$, $y = 8$	1.3 / 5.3	1.2 / 5.3	1.0 / 4.1	1.0 / 4.1
$x = 8$, $y = 8$	0.4 / 1.0	0.5 / 1.0	0.3 / 0.8	0.3 / 0.7

agreement between our sensitivity expression and the averaged raytracing results for all cases, see table 1.

From figure 3b it is clear that there are significant differences between the sensitivity of a single fixed collimator set-up and the average over 100 configurations. This is most pronounced close to the collimator, i.e. $z < 35$ mm in figure 3b. This confirmed that the precise location of the septa can have a clear influence on the sensitivity especially close to the collimator as one might expect. We can see from table 1 that for the fan beam collimator the maximum difference increased from 0.5% for the average over 100 configurations to 4.4% for a single configuration for the off axis line. For the cone beam example (see figure 4), the difference is less.

3.4. Septa penetration

As mentioned, in our derivation penetration of collimator septa was not considered as it was neither in the traditional derivation. Usually penetration is then included by replacing the collimator length L by an effective collimator length that depends on the attenuation coefficient of the collimator material at the gamma photon's energy (see section 2.4). For an initial analysis of the effect of penetration, we reran the raytracing simulation to include modelling of septa penetration. We calculated the difference between the raytracing simulation and the expression using either the physical length L, or the effective length L_e in (11). From the results in table 2, we see that using an effective length reduces the differences between the averaged raytracing simulations and the analytical expression, but the differences are still larger than for the case without penetration (c.f. table 2). For example the mean difference in the on-axis sensitivity of the fan beam collimator improves from 1.5% to 0.9% when L_e is used instead of L, while without penetration modelling in the raytracer the difference is 0.5%.

3.4.1. Volumetric Sensitivity To analyse the conditions for which the old diverging formula is still a good approximation for calculating volumetric sensitivity, we looked

Table 3. Volumetric (average) sensitivity for a brain SPECT cone beam example (see section 2.4.1). Comparing (11), with the traditional diverging formula 10

Focal length (mm)	Sensitivity from (11) (%)	Sensitivity from (10) (%)	Difference (%)
150 mm	0.048	∞	∞
200 mm	0.057	∞	∞
250 mm	0.062	0.160	158
300 mm	0.063	0.100	60
350 mm	0.061	0.075	24
400 mm	0.057	0.062	9.8

at an example for volumetric sensitivity as described in section 2.4.1. The sensitivity was calculated on a grid with voxel size of 1 mm, and then averaged over a spherical volume-of-interest (VOI) with diameter of 200 mm . The results are listed in table 3. If the focal point is in the centre of the VOI (focal length 150 mm), the diverging expression does not produce a finite answer. On the other hand, when the focal point is outside the VOI, i.e. the focal length is larger than 250 mm, there is no singularity in the VOI and a finite answer is produced also with the traditional diverging expression. However, it is clear from table 3 that although the traditional formula produces a finite answer, it can still be significantly off when the focus is outside the volume, e.g. for a focal length of 350 mm, which is 100 mm beyond the VOI, we still find an error of 24% in the average sensitivity in the VOI .

4. Discussion

We derived a non-diverging expression for the sensitivity of converging collimators which is valid over the whole field-of-view, contrary to earlier derived expressions. Our expression shows good agreement with raytracing simulation data. We showed that it agrees well (mean difference from 0.1% to 0.7 % and max difference from 0.4 to 5.6 %) with a raytracing simulation that was averaged over different configurations (different exact locations of the septa). Note that our sensitivity formula does not depend on the exact placement of the septa and from its derivation it is clear that it corresponds to a sensitivity averaged over different septa locations. As shown in figure 3, figure 4, and table 1, the sensitivity can be significantly influenced by the exact location of the septa and holes when the source is placed close to the collimator; for a source right above a hole more photons are detected than when the source is just above a septum. This is true not only for cone and fan beam, but also for the parallel hole collimators. One could in principle derive a formula in which the exact location of the septa is contained but this would become very complicated. Therefore, all analytical sensitivity expressions represent an average over slightly different geometries. One should however be aware that in the case an exact collimator response is required (e.g. in iterative image reconstruction) the exact septa/ hole location may need to be considered (Formiconi, 1998).

In our derivation, penetration of collimator septa is neglected. Including septal penetration into the collimator's response function would make the derivation tremendously more complex and we are not aware of any sensitivity calculation into which this is fully taken into account, even not for the simpler case of parallel hole collimators . The common way to include penetration is to replace the actual physical

collimator length by an effective hole length as we have also done.

In the derivation the only approximations made are the averaging step over the septa positions, and the mentioned neglected septal penetration. No other approximations were used as we evaluated the integral fully. The fact that on the collimator axis the numerical agreement is within 1/10000th of the separately derived and differently formulated expression from Accorsi and Metzler (2006), and the fact that in special cases it reduces to other previously known formulas makes us confident that we didn't make any mistakes in our calculation. Therefore, we believe the remaining differences between our expression and the raytracing simulations can be explained by discretization errors in the simulation. Firstly, the collimator volume in our raytracer is represented with finite voxels. Especially for thin septa, the continuous septa are challenging to accurately represent with cubic voxels. In our simulations we assume a voxel size of 0.05 mm while septa had a thickness of 0.2 and 0.3 mm. Smaller voxels would lead to prohibitively large collimator volumes, as the collimator volumes used in this paper took already 19 GiB to store. Secondly, the detector is modelled with finite pixels, which can be partially covered by septa while the raytracer only traces to the centre of a pixel. Lastly the averaging over the different septa locations was done using 100 configurations. Although, one expects the effect on sensitivity to be relatively smooth as function of the septa locations, and 10 samples in each direction should suffice, a small error is introduced here as well.

The traditional sensitivity formula for parallel hole collimators, on which the first fan and cone beam expressions are based, contain a factor describing effects of different hole shapes and patterns. This factor is usually denoted with k or K (Anger, 1967; Cherry et al., 2003). The traditional diverging expressions for converging collimators include the same factor. In their paper about the non-diverging axial formula for converging collimators, Accorsi and Metzler (2006) provide a more extensive description of the effect of hole shape and they derived additional correction factors that can be used to convert sensitivity formulas of square holes to other hole shapes, such as round or hexagonal holes. Such factors can also be included in our expressions although it is besides the scope of this paper to test their accuracy.

In literature, different definitions of the parameters for converging hole collimators can be found. We decided to keep the hole area constant at the object side of the collimator as is commonly done (Tsui and Gullberg, 1990; Accorsi and Metzler, 2006), while others like Formiconi (1998) kept the bore width (the distance between septa measured perpendicular to each hole's axis) constant at the object side of the collimator, thereby making the areas of the holes at the collimator surface larger towards the collimator edges, as in the edges in the x and y directions.

Note that precise manufacturing of converging collimators is a difficult process which has caused constraints in collimator design, as for example thin septa are very hard to produce. In recent years new technologies like 3D printing have emerged that allow more challenging designs to be manufactured (Van Audenhaege et al., 2015; Pato et al., 2015) that may better exploit the advantages of strongly focusing collimators. Therefore, a new look at the possibilities of converging collimators might be worthwhile and correct sensitivity expressions for such collimators are then desirable.

5. Conclusions

We derived a new expression for the sensitivity of converging collimators. Contrary to known sensitivity formulas, our formula is valid over the full field-of-view and does

not diverge near the focus. It can thus be applied to accurately determine sensitivity near the focus of converging collimators.

6. Acknowledgement

This work is supported by the Dutch Organization for Scientific Research (NWO) under the VIDI grant 12371 Focused imaging of tumors.

Appendix A. Figure

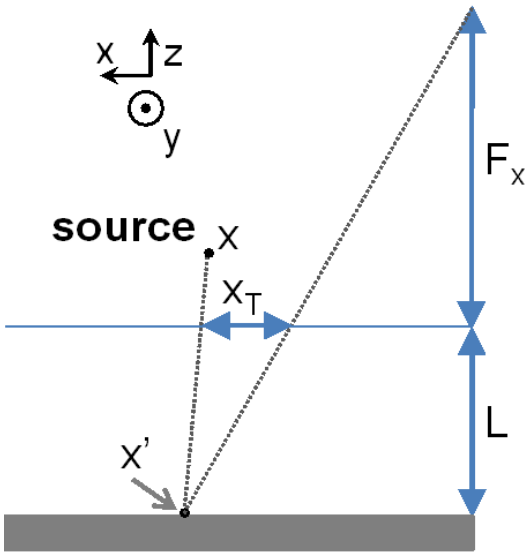

Figure A1. Schematic overview of the definition of $\mathbf{r}_T = (x_T, y_T)$. Illustrated are dashed lines from the source to the current integration point x', from the focus to the current integration point x', the distance between these two lines on the collimator surface x_T. While this illustration is in two dimensions, y_T can be illustrated likewise.

References

Accorsi, R. and Metzler, S. D. (2006). Non-diverging analytic expression for the on-axis sensitivity of converging collimators: analytic derivation, *Phys Med Biol* **51**(21): 5675–96.
URL: https://doi.org/10.1088/0031-9155/51/21/019

Anger, H. O. (1967). Radioisotope cameras, *in* G. J. Hine (ed.), *Instrumentation in Nuclear Medicine*, Vol. 1, Academic Press, New York, NY, USA, chapter 19, pp. 485–552.

Beekman, F. J. (2001). Apparatus for making tomographic images. US Patent 6,324,258.

Beekman, F. J., Kamphuis, C., Hutton, B. F. and van Rijk, P. P. (1998). Half-fanbeam collimators combined with scanning point sources for simultaneous emission-transmission imaging, *Journal of Nuclear Medicine* **39**(11): 1996–2003.
URL: *http://jnm.snmjournals.org/content/39/11/1996.short*

Cherry, S. R., Sorenson, J. A. and Phelps, M. E. (2003). *Physics in Nuclear Medicine*, 3rd edn, Saunders, Philadelphia, PA, USA.

Formiconi, A. R. (1998). Geometrical response of multihole collimators, *Physics in Medicine and Biology* **43**(11): 3359–79.
URL: *http://stacks.iop.org/0031-9155/43/i=11/a=013*

Goorden, M. C., Rentmeester, M. C. M. and Beekman, F. J. (2008). Theoretical analysis of multi-pinhole brain spect, *IEEE Nuclear Science Symposium Conference Record*, pp. 4036–4038.
URL: *https://doi.org/10.1109/NSSMIC.2008.4774170*

Gradshteyn, I. and Ryzhik, I. (2014). *Table of Integrals, Series, and Products*, Elsevier Science.
URL: *https://books.google.nl/books?id=F7jiBQAAQBAJ*

Gullberg, G. T., Christian, P. E., Zeng, G. S. L., Datz, F. L. and Morgan, H. T. (1991). Cone beam tomography of the heart using single-photon emission-computed tomography, *Investigative Radiology* **26**(7): 681–688.
URL: *https://doi.org/10.1097/00004424-199107000-00014*

Gullberg, G. T., Zeng, G., Christian, P. E., Tsui, B. and Morgan, H. T. (1991). Single photon emission computed tomography of the heart using cone beam geometry and noncircular detector rotation, *Progress in clinical and biological research* **363**: 123–138.

Gunter, D. L. (2004). Collimator design for nuclear medicine, *in* M. N. Wernick and J. N. Aarsvold (eds), *Emission tomography: the fundamentals of PET and SPECT.*, Elsevier Academic, San Diego, London, pp. 153–68.

Hawman, P. C. and Haines, E. J. (1994). The cardiofocal collimator: a variable-focus collimator for cardiac spect, *Physics in Medicine and Biology* **39**(3): 439.
URL: *http://iopscience.iop.org/article/10.1088/0031-9155/39/3/011/pdf*

Jaszczak, R. J., Chang, L. T. and Murphy, P. H. (1979). Single photon emission computed tomography using multi-slice fan beam collimators, *IEEE Transactions on Nuclear Science* **26**(1): 610–618.
URL: *http://ieeexplore.ieee.org/xpl/articleDetails.jsp?arnumber=4329698*

Jaszczak, R. J., Floyd, C. E., Manglos, S. H., Greer, K. L. and Coleman, R. E. (1986). Cone beam collimation for single photon-emission computed-tomography - analysis, simulation, and image-reconstruction using filtered backprojection, *Med Phys* **13**(4): 484–489.
URL: *http://dx.doi.org/10.1118/1.595854*

Jaszczak, R. J., Greer, K. L. and Coleman, R. E. (1988). Spect using a specially designed cone beam collimator, *Journal of Nuclear Medicine* **29**(8): 1398–1405.
URL: *http://jnm.snmjournals.org/content/29/8/1398.short*

Kamphuis, C. and Beekman, F. J. (1998). The use of offset cone-beam collimators in a dual head system for combined emission transmission brain spect: a feasibility

study, *IEEE Transactions on Nuclear Science* **45**(3): 1250–1254.
URL: http://ieeexplore.ieee.org/xpl/articleDetails.jsp?reload=true&arnumber=682011

Kemp, B. J., Prato, F. S., Nicholson, R. L. and Reese, L. (1995). Transmission computed tomography imaging of the head with a spect system and a collimated line source, *Journal of Nuclear Medicine* **36**(2): 328–335.
URL: http://jnm.snmjournals.org/content/36/2/328.short

Kijewski, M. F., Mller, S. P. and Moore, S. C. (1997). Nonuniform collimator sensitivity: Improved precision for quantitative spect, *Journal of Nuclear Medicine* **38**(1): 151–156.
URL: http://jnm.snmjournals.org/content/38/1/151.short

Li, J., Jaszczak, R. J., Van Mullekom, A., Scarfone, C., Greer, K. L. and Coleman, R. E. (1996). Half-cone beam collimation for triple-camera spect systems, *Journal of Nuclear Medicine* **37**(3): 498–502.
URL: http://jnm.snmjournals.org/content/37/3/498.short

Lowe, D., Truman, A., Kwok, H. and Bergman, A. (2002). Optimisation of the design of round-hole parallel collimators for ultra-compact nuclear medicine imaging, *Nuclear Instruments and Methods in Physics Research Section A: Accelerators, Spectrometers, Detectors and Associated Equipment* **488**(12): 428 – 440.
URL: http://www.sciencedirect.com/science/article/pii/S0168900202003923

Manglos, S. H., Bassano, D. A., Thomas, F. D. and Grossman, Z. D. (1992). Imaging of the human torso using cone-beam transmission ct implemented on a rotating gamma camera, *Journal of Nuclear Medicine* **33**(1): 150–156.
URL: http://jnm.snmjournals.org/content/33/1/150.short

Mather, R. L. (1957). Gamma-ray collimator penetration and scattering effects, *Journal of Applied Physics* **28**(10): 1200–1207.
URL: http://scitation.aip.org/content/aip/journal/jap/28/10/10.1063/1.1722607

Metz, C. E., Atkins, F. B. and Beck, R. N. (1980). The geometric transfer function component for scintillation camera collimators with straight parallel holes, *Physics in Medicine and Biology* **25**(6): 1059.
URL: http://stacks.iop.org/0031-9155/25/i=6/a=003

Moyer, R. A. (1974). A low-energy multihole converging collimator compared with a pinhole collimator, *Journal of Nuclear Medicine* **15**(2): 59–64.
URL: http://jnm.snmjournals.org/content/15/2/59.short

Park, M.-A., Kijevvski, M. F. and Moore, S. C. (2003). Evaluation of ultra-short focusing cone-beam collimators for spect brain imaging, *Nuclear Science Symposium Conference Record, 2003 IEEE*, Vol. 3, pp. 1865–1867 Vol.3.
URL: http://ieeexplore.ieee.org/xpl/articleDetails.jsp?arnumber=1352242

Park, M.-A., Moore, S. C. and Kijewski, M. F. (2005). Brain spect with short focal-length cone-beam collimation, *Medical Physics* **32**(7): 2236–2244.
URL: http://dx.doi.org/10.1118/1.1929208

Pato, L. R. V., Vandenberghe, S., Zedda, T. and Holen, R. V. (2015). Parallel-hole collimator concept for stationary spect imaging, *Physics in Medicine and Biology*

60(22): 8791.
URL: http://stacks.iop.org/0031-9155/60/i=22/a=8791

Rentmeester, M. C., van der Have, F. and Beekman, F. J. (2007). Optimizing multi-pinhole spect geometries using an analytical model, *Phys Med Biol* **52**(9): 2567–81.
URL: http://www.ncbi.nlm.nih.gov/pubmed/17440253

Siddon, R. L. (1985). Fast calculation of the exact radiological path for a three-dimensional ct array, *Medical Physics* **12**(2): 252–255.
URL: http://dx.doi.org/10.1118/1.595715

Ter-Antonyan, R., Jaszczak, R. J., Greer, K. L., Bowsher, J. E., Metzler, S. D. and Coleman, R. E. (2009). Combination of converging collimators for high-sensitivity brain spect, *Journal of Nuclear Medicine* **50**(9): 1548–1556.
URL: http://jnm.snmjournals.org/content/50/9/1548.abstract

Tsui, B. M., Gullberg, G. T., Edgerton, E. R., Gilland, D. R., Perry, J. R. and McCartney, W. H. (1986). Design and clinical utility of a fan beam collimator for spect imaging of the head, *J Nucl Med* **27**(6): 810–9.
URL: http://jnm.snmjournals.org/content/27/6/810.short

Tsui, B. M. W. and Gullberg, G. T. (1990). The geometric transfer-function for cone and fan beam collimators, *Phys Med Biol* **35**(1): 81–93.
URL: https://doi.org/10.1088/0031-9155/35/1/008

Van Audenhaege, K., Van Holen, R., Vandenberghe, S., Vanhove, C., Metzler, S. D. and Moore, S. C. (2015). Review of spect collimator selection, optimization, and fabrication for clinical and preclinical imaging, *Medical Physics* **42**(8): 4796–4813.
URL: http://scitation.aip.org/content/aapm/journal/medphys/42/8/10.1118/1.4927061

van Roosmalen, J., Goorden, M. C. and Beekman, F. J. (2015). Optimization of a high resolution focussed molecular breast tomosynthesis device, *Nuclear Science Symposium and Medical Imaging Conference (NSS/MIC)*.

Walrand, S., van Dulmen, A., van Rossem, H. and Pauwels, S. (2002). Acquisition of linograms in spet: implementation and benefits, *European Journal of Nuclear Medicine and Molecular Imaging* **29**(9): 1188–1197.
URL: http://dx.doi.org/10.1007/s00259-002-0862-x

Wang, B., van Roosmalen, J., Pit, L., van Schie, M., Beekman, F. J. and Goorden, M. C. (submitted). Voxelized ray-tracing simulation dedicated to multi-pinhole molecular breast tomosynthesis, *Physics in Medicine and Biology* .

Weinmann, A. L., Hruska, C. B. and O'Connor, M. K. (2009). Design of optimal collimation for dedicated molecular breast imaging systems, *Medical Physics* **36**(3): 845–856.
URL: https://doi.org/10.1118/1.3077119